Available online at www.sciencedirect.com

ScienceDirect

Nuclear Data Sheets 119 (2014) 162–164

Nuclear Data Sheets

www.elsevier.com/locate/nds

# Neutron Capture Measurements and Resonance Analysis of Dysprosium

Y.R. Kang,[1] M.W. Lee,[1] T.I. Ro,[2] G.N. Kim,[3,*] Y. Danon,[4] and D. Williams[4]

[1] *Research Center, Dongnam Inst. of Radiological & Medical Sciences, Busan 619-953, Republic of Korea*
[2] *Department of Physics, Dong-A University, Busan 604-714, Republic of Korea*
[3] *Department of Physics, Kyungpook National University, Daegu 702-701, Republic of Korea*
[4] *Gaerttner LINAC Center, Rensselaer Polytechnic Institute Troy, New York 12180-3590, USA*

The electron linear accelerator facility at the Rensselaer Polytechnic Institute was used to measure neutron capture yields of dysprosium with the time-of-flight method in the neutron energy region from 10 eV to 1 keV. The neutron capture experiments were made at a flight path length of 25.5 m with a 16-section NaI multiplicity detector. High purity isotopic samples of $^{161}$Dy, $^{162}$Dy, $^{163}$Dy, $^{164}$Dy as well as one natural dysprosium sample with thickness of 0.508 mm were used in this measurement. Resonance parameters were extracted from the data using simultaneous fit with the multilevel R-matrix Bayesian code SAMMY 8.0. New resonances are proposed, and other resonances previously identified in the literature have been revised. The present results are compared with other evaluated values of ENDF/B-VII.1 and JENDL 4.0.

## I. INTRODUCTION

Dysprosium has many uses in the field of nuclear reactor system due to a very large thermal neutron absorption cross-section. The ability to absorb neutrons readily without swelling or contracting over time as well as its high melting point makes dysprosium alloyed with special stainless steels attractive for control in nuclear reactor [1]. Dysprosium is also a fission product from the thermal fission of $^{235}$U, $^{233}$U, and $^{239}$Pu. The accumulation of fission products in the reactor core increase with the burn-up of the nuclear fuel and the poison effect becomes more important. In addition, it is difficult to separate from minor actinides such as and other minor actinides. If spent nuclear fuel is to be reprocessed and it is desired to burn up the minor actinide burning core [2]. Therefore, it is necessary to understand dysprosium's effect on the neutron population over all energy regions in a nuclear reactor system, where it is in the capacity of a fission product poison or a neutron absorbing control rod. We present the results of neutron capture experiments on four important Dy isotopes. The experiments were performed at the electron linear accelerator (LINAC) facility of the Rensselear Polytechnic Institute (RPI) in the neutron energy region from 10 eV to 1 keV. Resonance parameters were extracted by fitting the neutron capture data using the SAMMY multilevel R-matrix Bayesian code [3]. A more detailed description of the present measurement and analysis is given in Reference [4].

## II. EXPERIMENTAL SETUP

Pulses of neutrons are generated via photoneutron reactions when the 60 MeV electron beam from the RPI LINAC impinges on a water-cooled tantalum target. The description of the water-cooled tantalum target, the capture detector, and the data acquisition system was given in detail elsewhere [4, 5], so only a brief description is given in the present paper. The bare-bounce neutron target (BBT) used for this measurement is unique in that the tantalum plates are mounted off the neutron beam axis. A 2.5-cm-thick polyethylene moderator is mounted adjacent to the tantalum plates and centered on the neutron beam axis. The moderator effectively slows down the fast neutrons generated in the target through collisions with hydrogen and emits the neutrons at a lower energy. These moderated neutrons are then collimated as they drift down an evacuated flight tube to the sample and detector. In order to remove low energy neutrons from previous pulses, a 0.8-cm-thick $^{10}B_4C$ overlap filter was inserted in the neutron beam line. The neutron energy for a detected event is determined from the flight time of the neutron using the time-of-flight (TOF) technique, and from the precise knowledge of the flight path length. The overall dead time of the signal-processing electronics was set at 1.125 $\mu$s for capture measurements. During operation of the experiment, data were transferred from the TOF analyzer to the computer memory via direct memory access. The data-taking software is completely menu driven and controls the sample changer, sorts the data into individual spectra, and provides on-line display of the data being accumulated. A description of data

* Corresponding author: gnkim@knu.ac.kr

http://dx.doi.org/10.1016/j.nds.2014.08.045

taking computer system, data file structure, and data reduction process is available in elsewhere [4].

The capture detector is a $\gamma$-detector containing 20 $\ell$ of NaI(Tl) divided into 16 optically isolated segments. The cylinder is split across its axis into two rings, with each ring divided into eight equal pie-shaped segments. Each segment is hermetically sealed in an aluminum can and is connected to a photomultiplier tube. The neutron beam was collimated to a diameter of 4.76 cm. Neutrons that scatter from the sample are absorbed by a hollow cylindrical liner fabricated of $^{10}B_4C$ ceramic to reduce the number of scattered neutrons reaching the detector. The detector system discriminates against the 478-keV $\gamma$-ray from $^{10}$B(n;$\alpha$,$\gamma$) reactions. The capture detector used for the present experiment was located at the east beam tube at a flight path of 25.569±0.006 m from the bare-bounce target. The flight path length was determined from measurements of precisely known $^{238}$U resonances. The efficiency of the capture detector is assumed to be the same for all Dy isotopes. Four isotopically-enriched Dy metallic samples were used in order to reduce the overestimate of the capture yield due to the hydroscopic property in oxide power samples. One elemental Dy sample with thickness of 0.508 mm was also used. The isotopic contents of the Dy samples used in the experiments are listed in Table I. The isotopic abundances of the elemental samples are taken from Reference [6].

TABLE I. Isotopic Composition of Dysprosium Samples.

| sample | Isotopic Composition (%) | | | | | | |
|---|---|---|---|---|---|---|---|
| | $^{156}$Dy | $^{158}$Dy | $^{160}$Dy | $^{161}$Dy | $^{162}$Dy | $^{163}$Dy | $^{164}$Dy |
| $^{161}$Dy | 0.02 | 0.02 | 0.35 | 95.66 | 2.53 | 0.9 | 0.56 |
| $^{162}$Dy | <0.01 | <0.01 | 0.08 | 1.24 | 96.17 | 1.79 | 0.72 |
| $^{163}$Dy | <0.01 | <0.01 | 0.03 | 0.36 | 1.23 | 96.86 | 1.52 |
| $^{164}$Dy | <0.01 | <0.02 | 0.02 | 0.15 | 0.35 | 1.03 | 98.45 |
| $^{nat}$Dy | 0.06 | 0.10 | 2.34 | 18.9 | 25.5 | 24.9 | 28.2 |

The thickness of samples in atoms/barn are $(6.359 \pm 0.011) \times 10^{-4}$, $(6.445 \pm 0.015) \times 10^{-4}$, $(6.503 \pm 0.140) \times 10^{-4}$, $(6.196 \pm 0.690) \times 10^{-4}$, and $(16.304 \pm 0.013) \times 10^{-4}$ for $^{161}$Dy, $^{162}$Dy, $^{163}$Dy, $^{164}$Dy, and $^{nat}$Dy, respectively. The uncertainties in thickness of samples were propagated from multiple measurements of the sample. The diameter measurements are the dominant component of the uncertainties. All samples were mounted in aluminum sample cans. The thickness of aluminum on each of the front and rear faces of each sample was 0.38 mm. The influence of these sample cans, as well as all background, was measured by including empty sample cans in the capture measurements. In order to measure the flight path length and to calibrate the neutron energy, we also used a $^{238}$U sample. Samples were precisely positioned at the center of the capture detector by a computer-controlled sample changer.

## III. DATA REDUCTION AND ANALYSIS

Data taking and data reduction techniques for the experiment at the RPI LINAC are described in References [4]. A minimum of 100-keV $\gamma$-energy was required in a detector segment to be counted. Data were recorded as capture events only if the total energy deposited in all 16 segments exceeded 1 MeV. The data were recorded as scattering events if the total deposited $\gamma$-ray energy fell between 360 to 600 keV. This scattering energy region contains the 478-keV $\gamma$-ray emitted from the (n;$\alpha$,$\gamma$) reaction in the $^{10}B_4C$ annular detector liner. The large amount of TOF data collected in each capture measurement was subjected to statistical integrity checks to verify the stability of the electron LINAC, the capture detector, and associated beam monitors. Any data that failed the integrity test were eliminated. Next, the data were dead-time corrected, normalized to beam monitors, and summed. The background was determined using normalized data measured with an empty aluminum can mounted on the sample changer. This background was subtracted from the normalized and summed capture spectra. The 16 individual capture spectra were then summed into a single total spectrum. Processed TOF data are expressed as capture yield. The capture yield is defined as the number of neutron captures per neutron incident on the sample. Therefore, in addition to the Dy sample data, another set of data was needed to determine the energy profile of the neutron flux. The capture yield $Y_i$ in TOF channel $i$ was calculated by

$$Y_i = \frac{C_i - B_i}{K\phi_{smi}}, \tag{1}$$

where $C_i$ is dead-time-corrected and monitor-normalized counting rate of the sample measurement, $B_i$ is dead-time-corrected and monitor-normalized background counting rate, $K$ is product of the flux normalization factor and the detector efficiency $\phi_{smi}$ is smoothed, background-subtracted, and monitor-normalized neutron flux. The incident neutron flux shape was determined by mounting a 2.54-mm-thick, 97.9 wt % enriched $^{10}B_4C$ sample in the sample changer and adjusting the total energy threshold to record the 478-keV $\gamma$-rays from neutron absorption in $^{10}$B. Capture data were not used below 10 eV due to excessive background. Resonance parameters, neutron width $\Gamma_n$, radiation width $\Gamma_\gamma$, and resonance energy $E_0$, were extracted from the Dy capture data sets using the SAMMY multilevel R-matrix Bayesian code [3]. The present measurements assumed the same spin assignments as ENDF/B-VII.1 [7] for all resonances analyzed. As a starting point, the SAMMY fits Dy parameters from the ENDF/B-VII.1 parameters in the energy region of 10 to 1 keV. In this experiment, we have four enriched Dy samples and one natural Dy sample. Resonance parameters of $^{156}$Dy and $^{158}$Dy were fixed to ENDF/B-VII.1 values and not varied for all data because of its low abundance (0.06% and 0.10%). When

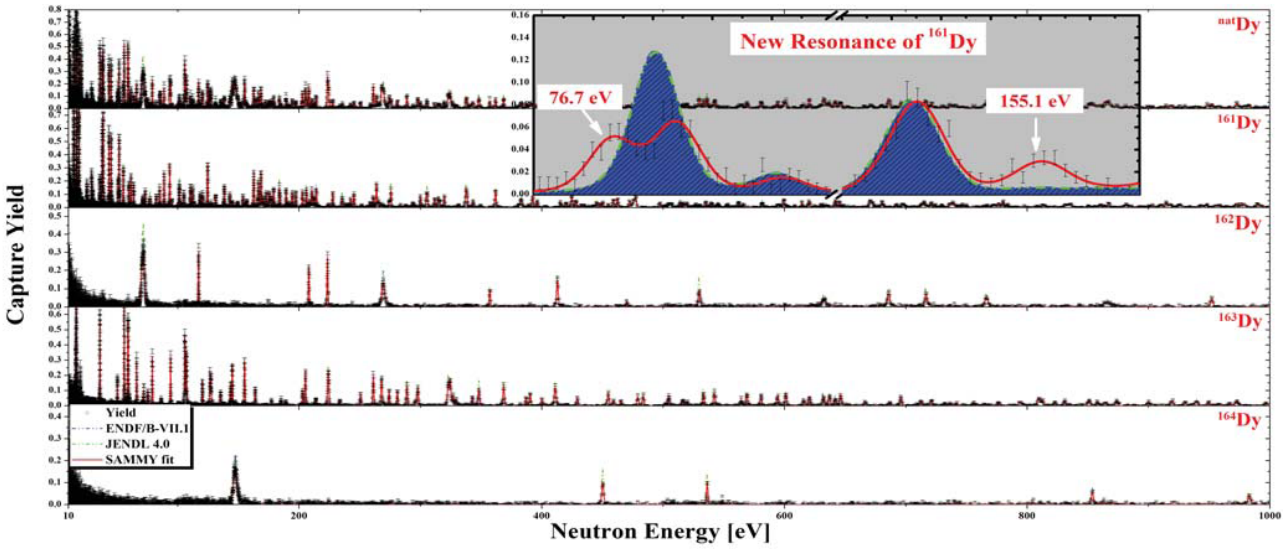


FIG. 1. An overview of capture data used in the energy region.

no further improvements in the fit were apparent and the resonance parameters remained unchanged relative to the previous iteration, the parameters were deemed final. The SAMMY code was then used to calculate capture yield curves based on these final resonance parameters to compare with the experimental data from each Dy sample. We also examined each resonance listed in ENDF/B-VII.1 to check whether it present in the data. If it did not look like a real resonance peak, It was removed the resonance from parameter file.

## IV. RESULTS AND CONCLUSIONS

Resonance parameters were extracted from capture data sets for Dy isotopes using the multilevel R-matrix Bayesian code SAMMY. The analysis included Doppler broadening, resolution broadening, and multiple scattering correcting of capture data. The present measured resonance parameters were determined using the capture yields for four enriched Dy isotopic samples and a natural sample. Figure 1 shows data from one natural Dy sample and four enriched Dy isotopes, and calculated curves for them, using the SAMMY program. We observed 27, 85, 23, 34, and 16 new resonances for $^{160}$Dy, $^{161}$Dy, $^{162}$Dy, $^{163}$Dy, and $^{164}$Dy isotopes not listed in ENDF/B-VII.1, respectively. Seven resonances from $^{161}$Dy isotope, one resonance from $^{163}$Dy isotope respectively, and three resonances from $^{164}$Dy isotope listed in ENDF/B-VII.1 have been discarded because the present measurements did not support their existence.

The present resonance parameters are compared with other evaluated values of ENDF/B-VII.1 and JENDL 4.0 [8]. The experimental data and resonance parameters are a significant improvement over previous measurements. The detailed list of resonance parameters for Dy isotopes are available and will be given in a future publication.

*Acknowledgements:* This research partly was supported by the National Research Foundation of Korea (NRF) through a grant provided by the Korean Ministry of Education, Science & Technology (MEST) in 2012 (Projects No. 2012-0007305), and by the National R & D Program through the Dong-nam Institute of Radiological & Medical Sciences (DIRAMS) funded by the Ministry of Education, Science and Technology (50491-2013)

[1] D. R. Lide, CRC Handbook of chemistry and physics 88th Edition, The Chemical Rubber Company (2008).
[2] M. Satoshi *et al.*, J. Nucl. Sci. Technol. **36**, 493 (2006).
[3] N.M. Larson, Updated Users Guide for SAMMY: Multilevel R-Matrix Fits to Neutron Data Using Bayes Equations, Report ORNL/TM-9179/R8 (2008).
[4] G. Leinweber *et al.*, Nucl. Sci. Eng. **164**, 287 (2010).
[5] R.W. Hockenbury *et al.*, Phys. Rev. **4**, 1746 (1969).
[6] E.M. Baum *et al.*, Chart of the Nuclides 17th ed., Knolls Atomic Power Laboratory (2009).
[7] M.B. Chadwick *et al.*, Nucl. Data Sheets **112**, 2887 (2011).
[8] K. Shibata *et al.*, J. Nucl. Sci. Technol. **48**, 1 (2011).